THE JOURNAL OF PHYSICAL CHEMISTRY A

Article

pubs.acs.org/JPCA

Photoactive High Explosives: Linear and Nonlinear Photochemistry of Petrin Tetrazine Chloride

Margo T. Greenfield, Shawn D. McGrane, Cindy A. Bolme, Josiah A. Bjorgaard, Tammie R. Nelson, Sergei Tretiak,* and R. Jason Scharff*

Los Alamos National Laboratory, Los Alamos, New Mexico 87545, United States

Supporting Information

ABSTRACT: Pentaerythritol tetranitrate (PETN), a high explosive, initiates with traditional shock and thermal mechanisms. In this study, the tetrazine-substituted derivative of PETN, pentaerythritol trinitrate chlorotetrazine (PetrinTzCl), is being investigated for a photochemical initiation mechanism that could allow control over the chemistry contributing to decomposition leading to initiation. PetrinTzCl exhibits a photochemical quantum yield (QY_{PC}) at 532 nm not evident with PETN. Using static spectroscopic methods, we observe energy absorption on the tetrazine (Tz) ring that results in photodissociation yielding N_2, Cl−CN, and Petrin−CN as the major photoproducts. The QY_{PC} was enhanced with increasing irradiation intensity. Experiment and theoretical calculations imply this excitation mechanism follows sequential photon absorption. Dynamic simulations demonstrate that the relaxation mechanism leading to the observed photochemistry in PetrinTzCl is due to vibrational excitation during internal conversion. PetrinTzCl's single photon stability and intensity dependence suggest this material could be stable in ambient lighting, yet possible to initiate with short-pulsed lasers.

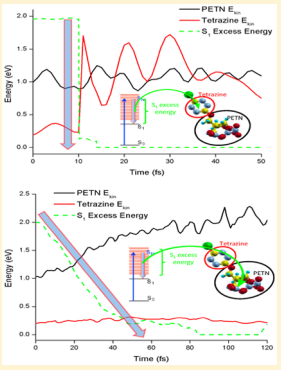

INTRODUCTION

Most high explosives (HEs) are not photoactive in the visible wavelength range; many are nitramines with large heats of combustion and white to off-white coloring, which characteristically absorb only in the ultraviolet (UV). The targeted design of photoactive high explosives can be obtained by tailoring/controlling the material's optical properties through synthesis. Tetrazine (Tz) is an ideal chromophore, due to its high heat of formation,[1] that can be synthetically linked to existing high explosives to optimize their photoactivity[2] without compromising their energetic performance.

Tetrazines are organic fluorophores with large heats of formation due to their C−N and N−N bonds.[1] They have a high electron affinity and are known as the most electron poor C−N heterocycles[3] and have a typically forbidden n−π^* transition located on the Tz ring.[4] They range in color from purple to red to orange depending upon how they are substituted. Substitution of Tz has been shown to increase thermal stability and give longer fluorescence lifetime and larger fluorescence quantum yield (QY_{fl}).[5,6] Tetrazines have been investigated for a wide range of applications such as protein folding,[7] antibacterial/antitumor,[8−10] sensors[11−15] and high-energy density materials such as high explosives.[2,16−18]

Current optical initiation mechanisms of conventional explosives are indirect thermal or shock processes that require high laser energies.[19−26] An optically active HE could open the door toward direct optical initiation through an excited state photodecomposition mechanism. Novel photoactive HEs could utilize multiphoton nonlinear excited state photochemical processes that lead to direct photoinitiation with some possibility of control over the reactive process. Ideal materials should have high photochemical yield, initiate on fast time scales, have highly exothermic reactions, and be photochemically accessible from commonly available laser wavelengths.

Herein we use a tetrazine-substituted derivative of pentaerythritol tetranitrate (PETN),[2] henceforth called PetrinTzCl, and associated materials PETN and tetrazine dichloride ($TzCl_2$) (see Figure 1) to establish the characterization and theoretical methods necessary for enhanced understanding of

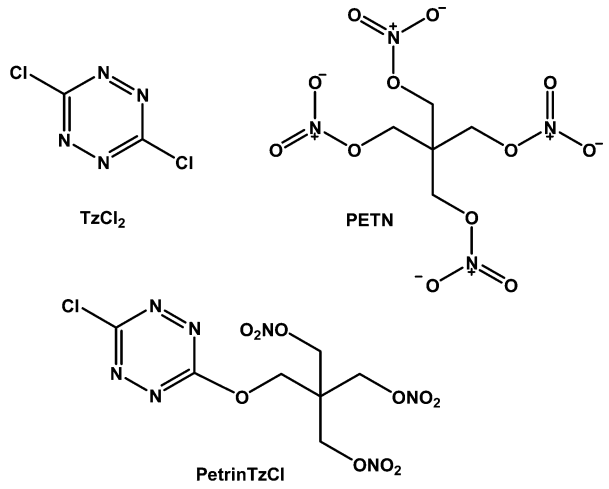

Figure 1. Chemical structures of $TzCl_2$, PETN, and PetrinTzCl.

Received: March 3, 2015
Revised: April 22, 2015
Published: May 7, 2015

DOI: 10.1021/acs.jpca.5b02092
J. Phys. Chem. A 2015, 119, 4846−4855

the material's photoactive response and associated energy transfer leading to photochemistry/photoproducts.

EXPERIMENTAL METHODS

To elucidate the photochemical quantum yield and associated photoproducts of PetrinTzCl, $TzCl_2$, and PETN, four experiments were completed: ultraviolet−visible (UV−vis) absorption, fluorescence quantum yield (QY_{fl}), photochemistry QY_{PC}, and mass spectrometry. The following paragraphs present the methods used in each experiment as well as methods used for the associated theoretical calculations.

UV−Vis. UV−vis absorption spectra of PetrinTzCl, $TzCl_2$, and PETN were obtained using an Agilent Technologies 8453 UV−vis spectroscopy system. Materials were ground with potassium bromide (KBr: Fisher Infrared grade) and pressed into 7 mm diameter pellets using an International Crystal Laboratories Port-A-Press. Pellets were further mounted to an Al mount with a 3 mm diameter hole, where the most optically clear region was selected for investigation. Concentrations were chosen such that a maximum 532 nm absorption was <0.5, and all pellets used in the intensity-dependent measurements were within ±5% of each other in peak absorbance. The number of molecules in a 3 mm diameter pellet for $TzCl_2$ was $\sim 5 \times 10^{17}$ molecules, PetrinTzCl was $\sim 5.3 \times 10^{16}$ molecules, and PETN was $\sim 2.3 \times 10^{17}$ molecules.

QY_{fl}. The QY_{fl} for PetrinTzCl was determined using the Rhodamine 6G perchlorate (Acros Organics laser grade 99.0% pure) in ethanol standard of $\Phi_f = 0.95$.[27] A 10 mm quartz cuvette was filled with the respective material and excited with a continuous wave 405 nm, 89.8 mW (±0.2 mW) diode laser. Emission spectra were obtained using a focusing lens attached to a fiber connected to a spectrometer (Ocean Optics USB 2000+). The 405 nm excitation laser was blocked from the collected emission spectra with a 405 nm notch filter. A 1.4×10^{-4} M solution of PetrinTzCl in acetone (Acros spectroscopic grade) was investigated to keep absorption <0.1. Acetone was chosen as the solvent due to PetrinTzCl's poor dissolution in ethanol.

QY_{PC}. The photochemical quantum yield, QY_{PC}, for continuous wave (CW) and pulsed 532 nm laser light was measured for the three materials. Molecular reactivity/photodegradation was measured via difference Fourier transform infrared (FTIR) spectra before and after photoirradiation. An FTIR spectrometer (Thermoscientific Nicolet iS 5) was modified to allow *in situ* CW or pulsed 532 nm irradiation and IR spectroscopy. A frequency-doubled diode pumped solid state (CNI model MGL-III-532) 532 nm CW laser and a Continuum Minilite (Q-switched, 5.7 ns full width at half-maximum (FWHM), ≤15 Hz pulsed 532 nm) laser were utilized to irradiate the materials. Pulsed 532 nm power was adjusted through a waveplate and polarizer. Both lasers were sent through a telescoping lens system to optimize the beam profile to a Gaussian configuration for consistent intensity/power irradiation with 2 mm FWHM.

Mass Spectrometry. A Stanford Research Systems residual gas analyzer (RGA-200) quadrupole mass spectrometer was employed to measure the gaseous photoproducts from PetrinTzCl, $TzCl_2$, and PETN under CW (74 mW average power) and pulsed (64 mW average power, 15 Hz) 532 nm laser irradiation. Sample pellets (7 mm diameter) were prepared as described in the UV−vis section and placed within a vacuum cell. Samples were evacuated to $<10^{-6}$ Torr using a Varian turbo-V70 pump, and mass spectra were obtained before and during laser irradiation, while continuously pumping the cell. Continuous pumping provided the highest level of background stability. Mass spectra from 1 to 200 mass/charge ratio were acquired every 40 s, with three scans averaged. Mass spectra were compared to the NIST Chemistry WebBook.[28]

COMPUTATIONAL METHODS

Linear and Nonlinear Optical Spectra. Quantum chemical calculations of optical spectra were performed with the Gaussian 03 and 09 software packages.[29,30] Following the method of Masunov and Tretiak,[31] optimized ground state geometries were calculated at the HF/6-31+G* level, and vertical excitation energies were calculated using time-dependent density functional theory (TD-DFT) at the B3LYP/6-31G* level. When compared to experimental data HF geometries are expected to be less accurate than some DFT geometries,[32] but a combination of HF geometries with TD-B3LYP approach produces consistent results for calculations of linear and nonlinear optical spectra across a wide range of molecular sizes.[33] Transition dipoles between the first and higher lying excited states were calculated using the collective electronic oscillator (CEO) formalism.[34]

To simulate the sequential absorption spectrum from the first excited state to higher excited states, the transition energies were broadened by a Gaussian function with FWHM of 0.05 eV. The resulting peaks were then weighted by the oscillator strengths calculated from the transition dipoles and summed, after which the total spectrum was normalized. A similar method was used to simulate the absorption spectrum for ground to excited state transitions using the corresponding oscillator strengths.[31] The nonlinear two-photon absorption (TPA) cross section was calculated in units of Goeppert−Meyers (GMs). The methods for this calculation were extensive and are detailed in ref 31.

Nonadiabatic Excited State Molecular Dynamics. The excited state dynamics of $TzCl_2$ and PetrinTzCl were explored using the previously developed nonadiabatic excited state molecular dynamics (NA-ESMD) framework described in detail elsewhere.[35−39] Briefly, the NA-ESMD approach combined the fewest switches surface hopping (FSSH) method with semiempirical Austin model 1 (AM1) and configuration interaction singles (CIS) description of the excited states[40] with on the fly calculation of the electronic energies, gradients, and nonadiabatic coupling vectors for the excited states. The electronic degrees of freedom were treated quantum mechanically, and the nuclear motions were treated classically. The probability for a quantum transition to another excited state depended on the strength of the nonadiabatic couplings calculated at each integration step along the trajectory. This approach allowed us to model the relaxation of a photoexcited wave packet from the excited state according to the following procedure. First, we ran molecular dynamics in the ground electronic state starting from the ground state optimized geometry for 300 ps with a time step of $\delta t = 0.5$ fs.[41,42] The system was then heated and allowed to equilibrate to a final temperature of 300 K during the first 10 ps using the Langevin thermostat[43] with a friction coefficient of 20.0 ps^{-1}. From the remaining 290 ps, we collected 190 configurations for $TzCl_2$ and 290 configurations for PetrinTzCl sampled at 1 ps intervals, which provided initial geometries and momenta for excited state simulations. Twenty $TzCl_2$ and 25 PetrinTzCl lowest energy electronic excited states and their oscillator strengths were then calculated for every configuration to determine

DOI: 10.1021/acs.jpca.5b02092
J. Phys. Chem. A 2015, 119, 4846−4855

energetic positions of the sequential two-photon state (located ~2.5 eV above the lowest energy excited S_1 state; see Results and Discussion). The initial excited state was chosen according to a Frank−Condon window defined as $g_\alpha = \exp[-T^2(E_{laser} - \Omega_\alpha)^2]$, where E_{laser} represents the excitation energy and Ω_α represents the computed energy of state α (expressed in units of fs^{-1}). The laser temporal profile was Gaussian $f(t) = \exp(-t^2/2T^2)$, T = 42.5 fs corresponding to a FWHM of 0.05 eV. The initial excitation was selected according to the relative values of g_α weighted by the oscillator strengths of each state. The NA-ESMD simulations were then started allowing internal conversion (IC) through coupled Born−Oppenheimer surfaces to be followed as the system returned to S_1. The swarm of independent trajectories was propagated via energy-conserving Newtonian dynamics for 1 ps ($TzCl_2$) and 4 ps (PetrinTzCl) using a classical time step of δt = 0.1 fs and three quantum steps per classical step. The quantum time step was further reduced by a factor of 40 to locate trivial unavoided crossings,[36] and the electronic decoherence was included by resetting the quantum coefficients following every attempted hop.[38]

RESULTS

Synthetically linking $TzCl_2$ to PETN changes the PETN from white to a bright pink/orange color enhancing the material absorption around 325 and 500 nm (see Figure 2). Note in

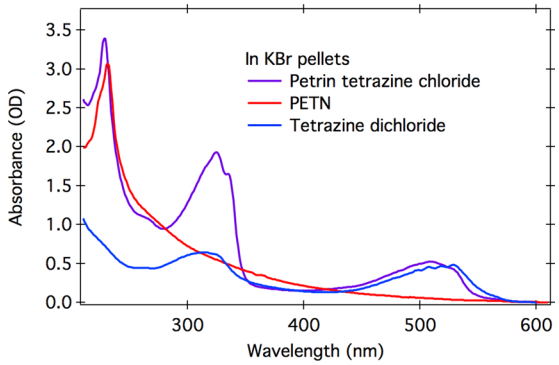

Figure 2. UV−vis spectra of PetrinTzCl, $TzCl_2$, and PETN in KBr pellets.

Figure 2 that the continuously increasing absorption with decreasing wavelength in PETN is due to scattering in the KBr pellet; scattering has been partially subtracted out by setting the absorption at 600 nm equal to zero. The n−π^* transition in PetrinTzCl has substantial absorption at 532 nm permitting excitation at an easily obtained commercial laser wavelength[4,44]

A 1.4 × 10^{-4} M solution of PetrinTzCl in acetone (Acros spectroscopic grade) exhibited a 0.18 ± 0.008 QY_{fl} (see emission spectrum Figure SI1). This moderate QY_{fl} is far larger than that observed for s-tetrazine, suggesting stabilization of the lowest energy electronic excited state for the substituted material.[45]

The number of molecules reacted per photon absorbed for CW and pulsed 532 nm laser irradiation was measured for PetrinTzCl, $TzCl_2$, and PETN. The QY_{PC} was directly calculated from the number of molecules irradiated within the 3 mm sample, the laser irradiance, and determination of the rate of molecular reactivity/photodegradation resulting from irradiation. The molecular reactivity was acquired via difference Fourier transform infrared (FTIR) spectra taken before and after photoirradiation at regular intervals.

Irradiated spectra were subtracted from initial reactant spectra to display the material vibrational changes that occurred due to photochemistry (difference spectra). Photoproduct vibrational spectra were determined by adding back a fractional amount, α, of the reactant spectra to the difference spectra such that negative peaks were removed. The concentration of initial material that had reacted, α, was determined in an automated process by minimizing the magnitude of the autocorrelation peak between the final product spectrum and the initial spectrum. If the trial α was too small, negative peaks would be apparent in the product spectrum, and there would be a negative autocorrelation peak. If α was too large, the autocorrelation peak would become positive. By calculating the magnitude of the autocorrelation as a function of α in steps of 0.25% material reacted, we determined the fraction reacted and the final product spectrum according to eq 1. Figure 3

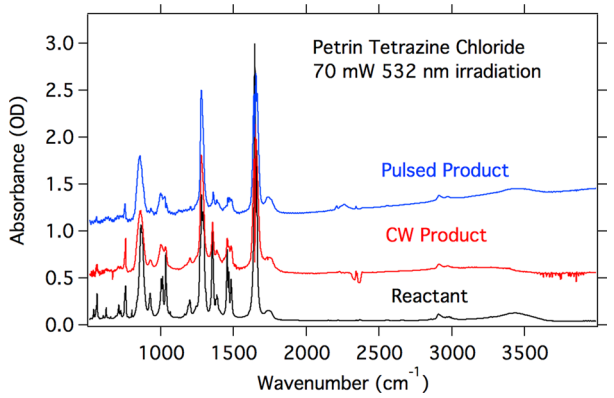

Figure 3. FTIR spectra of PetrinTzCl before (reactant) and photoproduct spectrum after 532 nm irradiation with CW (70 mW) and pulsed (70 mW, 15 Hz) light.

shows the reactant, CW product, and pulsed product spectra for PetrinTzCl. Specific peaks detailing the photochemistry will be discussed below, but first we utilize the spectra to determine the fraction of material that has reacted under different irradiation conditions.

$$\text{products} = \text{difference spectra} + \alpha\cdot\text{reactants} \quad (1)$$

To test the effect of intensity, new pellets of PetrinTzCl, $TzCl_2$, and PETN were subjected to various pulsed laser irradiances and compared to CW irradiation. The fraction of material reacted and product spectra were determined for each incremental increase in irradiation.

Figure 4 shows the resulting fraction of material reacted as a function of total energy absorbed and irradiance value. Both PetrinTzCl and $TzCl_2$ show a nonlinear/multiphoton intensity dependence[46] with 532 nm irradiation.[46] There was no measurable photoreaction of PETN following 10 000, 1.8 mJ, 5.7 ns pulses of 532 nm irradiation, due to its lack of absorption at that wavelength. The nonlinear effect of intensity on QY_{PC} for PetrinTzCl is shown in Figure 5. PetrinTzCl presented a 19× increase in QY_{PC} from 1.3 × 10^{-4} (CW) to 2.5 × 10^{-3} (pulsed) while $TzCl_2$ revealed a 54× increase from 7.1 × 10^{-3} (CW) to 0.39 (pulsed). As observed in Figure 2, 532 nm excites the first optically active electronic state resonantly, allowing sequential absorption of a second photon prior to relaxation with increasing probability as the intensity increases. This higher excited state appears to have a much greater photochemical reactivity, which is not surprising considering

DOI: 10.1021/acs.jpca.5b02092
J. Phys. Chem. A 2015, 119, 4846−4855

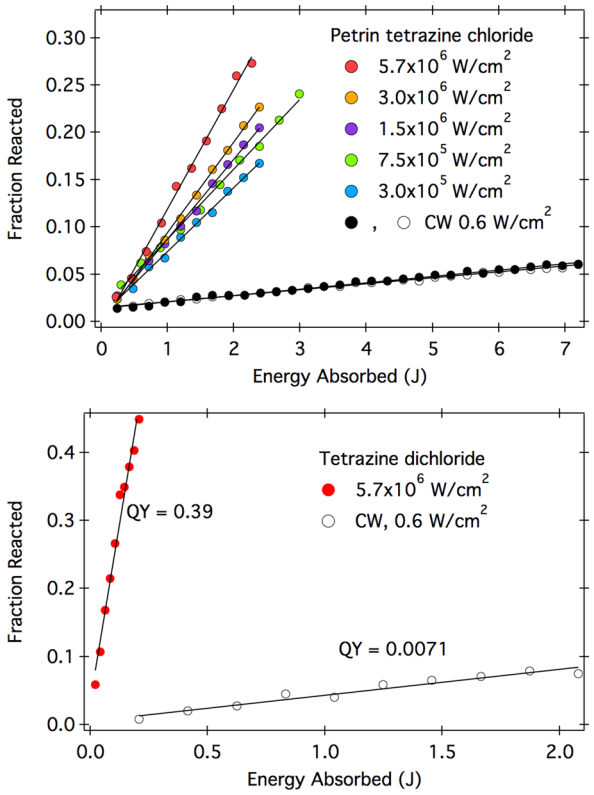

Figure 4. (top) Fraction of material photoreacted vs energy absorbed (J) for CW and increasing pulse irradiance for PetrinTzCl for 5.3 × 10^{16} molecules in the sample and 2.7 × 10^{18} photons/J. (bottom) Fraction of material photoreacted vs energy absorbed (J) for CW and maximum pulse irradiance for $TzCl_2$ for 5.0 × 10^{17} molecules in the sample and 2.7 × 10^{18} photons/J.

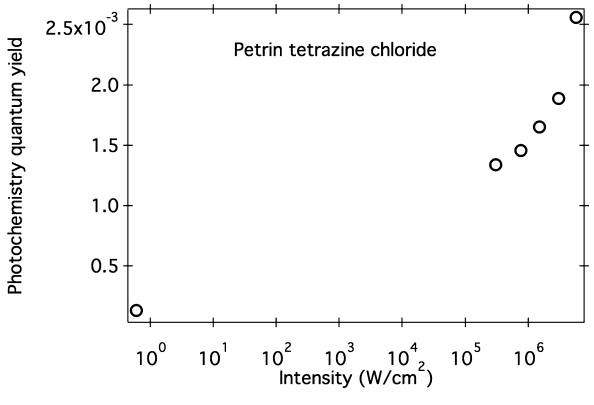

Figure 5. Nonlinear effect of photochemistry quantum yield vs intensity for PetrinTzCl.

the substantial increase in excess energy following absorption of two photons.

To determine the nature of the two-photon process, theoretical calculations were performed to differentiate between sequential absorption and nonlinear TPA. The standard absorption spectrum from the ground to excited state is calculated to be close in maximum to experiment, i.e. 570 nm, with an error of approximately 40 nm likely caused by dielectric environmental effects in experimental spectra that are not accounted for in theory. The calculated TPA cross section is relatively small with a maximum of less than 2 GMs for PetrinTzCl and below numerical precision for $TzCl_2$ (Figure SI2). Under the laser conditions of the experiment, the TPA was ∼6 orders of magnitude smaller than the one-photon absorption and can be neglected. The sequential absorption from the first excited state has significant absorption probability, which intersects with the ground-to-excited state absorption. In Figure 6, the relevant spectra are shown (one-photon absorption and sequential absorption from the first excited state). The highest sequential absorption probability is close to the 532 nm range and likely has a similar error (∼40 nm) as the calculated absorption probability from the ground state. This sequential absorption can lead to a total excess electronic energy of 4.5−5 eV above the ground electronic state, corresponding to the 6−8th B3LYP singlet excited states. These states cannot be optically excited by one-photon absorption (Figure 6, right panel) but can be optically excited by sequential absorption from the first excited electronic state (Figure 6, right panel). These states do not have significant two-photon absorption cross section (Supporting Information Table 1). It is concluded that sequential two-photon absorption is the primary method of excitation to higher energy excited states in these experiments.

In efforts to determine the energy transfer pathways associated with the photochemistry, additional analysis of the reactant and product spectra of PetrinTzCl, $TzCl_2$, and PETN was performed (Figure 7). PETN was not photoreactive at 532 nm and therefore had no product spectra while $TzCl_2$ presented negligible product spectra in the infrared that could be the result of CW irradiation induced photochemistry. In general, the product (CW or pulsed) spectrum of PetrinTzCl was similar to the reactant vibrational spectra. The most prominent distinction between the two was the overall decrease in peak intensity and some overall broadening. Specifically, the PetrinTzCl vibrations associated with the NO_2 stretch (1695 cm^{-1}), CH scissors (1483 cm^{-1}), CH_2 wag (1387 cm^{-1}), and O−N stretch (862) all remained after irradiation. There is also enduring evidence of the Tz ring contribution around 925 and 1198 cm^{-1}, although the 925 cm^{-1} vibration shifts slightly to 930 cm^{-1} in the product spectra.

A noted vibrational peak not evident in the $TzCl_2$ or PETN but present in the PetrinTzCl is the 1352 cm^{-1} peak. It is suggested that this vibrational peak is due to the C−O−C connection between the Tz and Petrin. The 1352 cm^{-1} vibrational peak decreases significantly in both CW and pulsed product spectra although a larger decrease is observed in the CW product spectra.

New vibrational peaks are observed in both the CW (2340 cm^{-1}) and pulsed (2209, 2250, and 2340 cm^{-1}) product spectra of PetrinTzCl and the pulsed product spectra of $TzCl_2$ (2209 cm^{-1}). The 2209 cm^{-1} peak is suggestive of a Cl−CN vibration, and the broad 2250 cm^{-1} peak is most likely due to Petrin−CN following previous mechanistic Tz decomposition results.[4,47,48] A sharp 2340 cm^{-1} peak is observed in both CW and pulsed PetrinTzCl but not in $TzCl_2$. This peak is likely from an isocyanate or nitrile species that is currently unidentified or potentially a complex with N_2 products.

The product spectra results demonstrate CN triple-bond formation, consistent with chemistry localized on the tetrazine moiety of PetrinTzCl. To further confirm this result, mass spectra of the gaseous photoproducts from PetrinTzCl and $TzCl_2$ under CW (74 mW) and pulsed (64 mW, 15 Hz) 532 nm laser irradiation were measured. Energy transfer leading to photodecomposition of the PETN portion of PetrinTzCl would lead to NO_2 and larger Petrin fragment gaseous photoproducts

DOI: 10.1021/acs.jpca.5b02092
J. Phys. Chem. A 2015, 119, 4846−4855

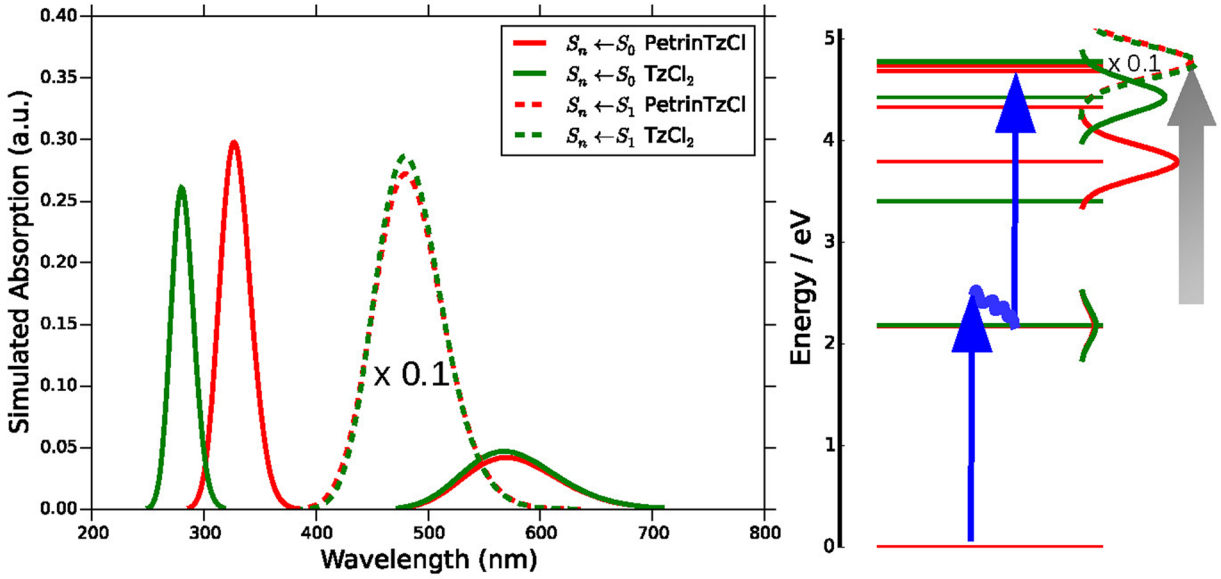

Figure 6. (left) Simulated ground to excited and excited to excited state absorption spectra for PetrinTzCl and $TzCl_2$. Ground to excited state absorption strength is multiplied by 10 for comparison. (right) Excitation energy diagram for PetrinTzCl and $TzCl_2$. Ranges of possible excitation according to the spectra on the right are shown with excited state absorption shifted to exhibit the higher lying states excited by this process.

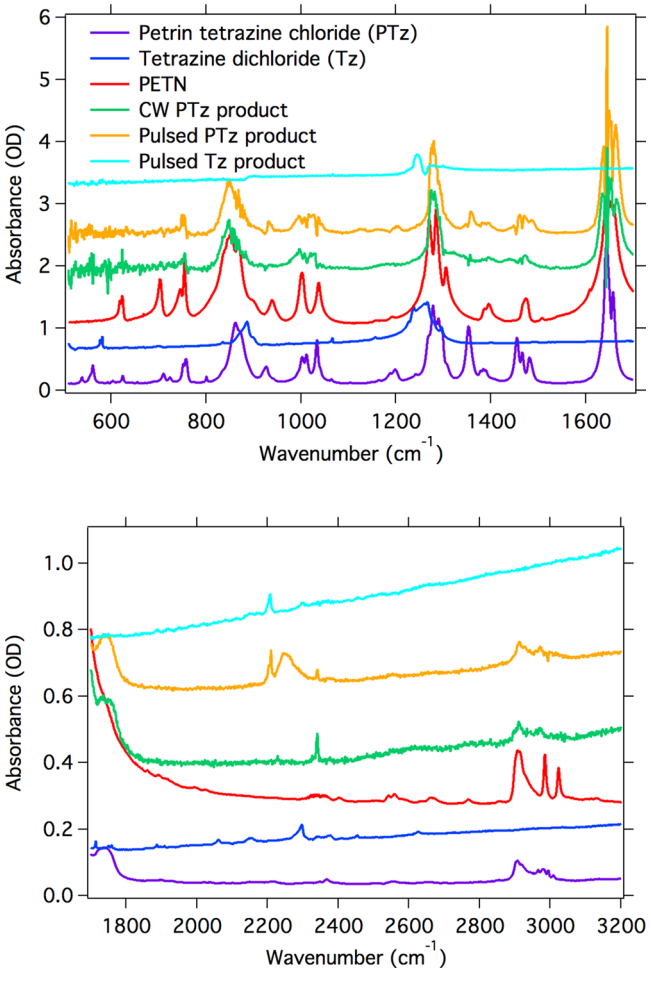

Figure 7. Reactant and product spectra for PetrinTzCl, $TzCl_2$, and PETN.

with prominent peaks expected at m/z of 46 and 76.[28] Figure 7 shows the mass spectroscopy results for the irradiated materials. Cl−CN, N_2, and Cl are detected in $TzCl_2$ for pulsed and CW conditions and for PetrinTzCl for only pulsed conditions. Cl−CN and Cl are not observed from CW irradiated PetrinTzCl, presumably due to the low QY_{PC}, but H_2O is detected, possibly from water absorbed in the KBr. There was no appreciable NO_2 or larger PETN subspecies (CH_2NO_3) present in the gas phase. There are some signatures of increased NO and CO_2 or N_2O production that would have to involve the PETN portion of PetrinTzCl.

DISCUSSION

An ideal photoactive HE material would exhibit a multiphoton/nonlinear QY_{PC}. This characteristic would increase explosive photoinitiation safety by preventing unwanted photodegradation due to single photon absorption of visible light from room/sunlight and low intensity laser light. It has been debated that the photochemistry of *s*-tetrazine falls within one of two photodecomposition mechanisms.[4,49,50] Mechanism one exhibits a one-photon absorption followed by IC with dissociation on the ground state via a concerted separation, as presented in reaction a. Mechanism two shows sequential two-photon absorption with dissociation through an excited state intermediate (X) as displayed in reaction b.

$$s\text{-Tz} \rightarrow 2\text{HCN} + \text{N}_2 \quad \text{(a)}$$

$$^1\text{Ag}\ s\text{-Tz} \rightarrow {}^1\text{B3}_\nu\ s\text{-Tz} \rightarrow {}^1\text{X}\ s\text{-Tz} \rightarrow 2\text{HCN} + \text{N}_2 \quad \text{(b)}$$

Further, it has been shown that the fluorescence, electrochemistry, and photochemistry depend upon the nature of the tetrazine derivative.[47,49] The measured nonlinear photochemical response of PetrinTzCl suggests that derivatizing Tz with the conventional high explosive PETN produces a photoactive material, which is more stable than tetrazine dichloride. It also suggests that the decomposition follows a sequential two-photon absorption mechanism. The following paragraphs discuss computational results, which substantiate cascaded sequential dissociation through an excited state

DOI: 10.1021/acs.jpca.5b02092
J. Phys. Chem. A 2015, 119, 4846−4855

intermediate of tetrazine dichloride and suggest a similar photochemical decomposition mechanism for PetrinTzCl.

Our experimental results exhibit PetrinTzCl undergoes decomposition through the Tz ring, while the Petrin moiety remains primarily intact. This occurs at a lower photochemical quantum yield than the analogous process in $TzCl_2$. The mechanism for this selective decomposition is a complex interplay of photoinduced pathways of internal conversion (IC) and/or intermolecular vibrational relaxation (IVR). The exact photophysical processes responsible for this cannot be clearly separated, given the current experimental data. From TD-B3LYP calculations, the excited states with significant sequential absorption probability are S_6, S_7, and S_8, with S_7 having ~10 times higher probability of absorption. Excited state geometry optimizations with an open shell formalism at the uB3LYP/6-31G* level were attempted but were not possible because of an apparent dissociation of $-NO_2$ from the Petrin moiety preventing convergence to a minimum-energy structure. This suggests an adiabatic photochemical dissociation of NO_2. However, no evidence of NO_2 production is present in Figure 8, although there is a signal for NO. It may be that NO is the final product present at long times related to the NO_2 reactions observed in simulation. The fact that the decomposition of the Petrin moiety is not experimentally observed may be due to rapid internal conversion (IC) involving multiple nonadiabatic transitions. To simulate these effects, nonadiabatic excited-state molecular dynamics was utilized.[35−39] To start these simulations, we have identified a single sequentially active state ($S_n \leftarrow S_1$) with large oscillator strength in the semiempirical AM1/CIS model chemistry used by NA-ESMD. This state is analogous to the state (S_7) obtained with TD-B3LYP and is localized on the tetrazine moiety.

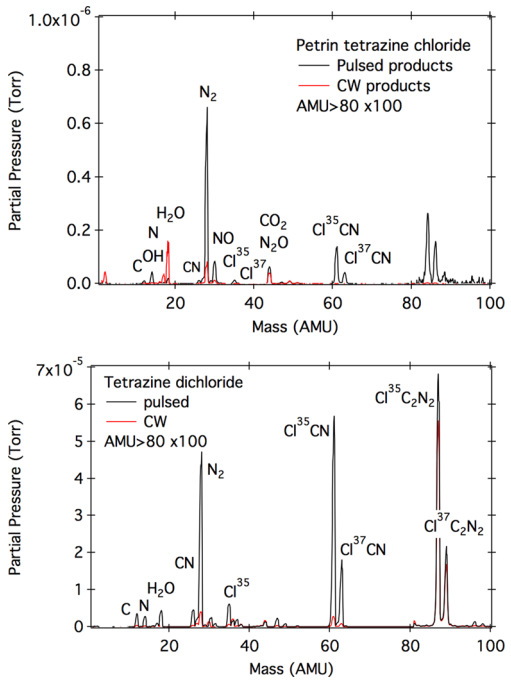

Figure 8. Mass spectra of CW and pulse irradiated PetrinTzCl (top) and $TzCl_2$ (bottom). The partial pressures of atomic mass units above 80 are multiplied by 100. Note that NO_2 (46 amu), NO_3 (62 amu), and CH_2NO_3 (76 amu) are missing from PetrinTzCl mass spectra, suggesting we are not directly observing Petrin dissociation.

Dynamic simulations predict ultrafast decomposition of the tetrazine ring in $TzCl_2$ with a quantum yield of 0.56 for the dissociation of a C−N bond. A second C−N bond dissociation resulting in the release of N_2 from the tetrazine ring was observed in a few of the trajectories exhibiting photochemistry. Notably, simulations of our trajectories typically stop after the first bond breakage due to the closed shell theoretical description of electronic excited states used here, which cannot describe radical anion intermediates. Because of this, we were not able to obtain the specific yield of the N_2 release or observe the final N−N bond cleavage in simulation. Molecular geometries collected along a representative NA-ESMD trajectory are shown in Figure 9. The ring-opening and loss of N_2 represent the first and second steps, respectively, of the cycloreversion process responsible for the production of Cl−CN and N_2 observed experimentally. For the PETN-substituted compound PetrinTzCl, C−N bond dissociation within the tetrazine ring was observed in a single trajectory out of 290 following 4 ps of NA-ESMD simulation time. Thus, the quantum yield for tetrazine photochemistry in PetrinTzCl is significantly reduced compared to $TzCl_2$ suggesting stability of the tetrazine moiety. NO_2 dissociation from the PETN functional group was observed with a simulated quantum yield of 0.06.

Molecular geometries along representative NA-ESMD trajectories for PetrinTzCl are shown in Figure 9. The tetrazine ring-opening and the Petrin NO_2 dissociation are shown in the middle and bottom panels, respectively.

These simulations support a photophysical mechanism responsible for the reactions in $TzCl_2$ and PetrinTzCl. As the system relaxes from the initial tetrazine localized sequentially excited electronic state ~2.5 eV above S_1 back to S_1 nonradiatively, the excess electronic energy from photo-excitation is dissipated as vibrational kinetic energy in the IC process.

Figure 10 shows the simulated nonadiabatic relaxation process in $TzCl_2$. The plot displays energies averaged over the ensemble of trajectories that display photochemistry. The S_1 excess electronic energy (green dashed line) is computed as the difference between the total potential energy and the lowest energy excited state S_1 energy, $E_{\mathrm{pot}}^{\mathrm{total}}(t) - E_1(t)$, and represents an ultrafast influx of the electronic energy into vibrations during IC. The S_1 excess energy goes to zero as the system relaxes back to S_1, and the relaxation is complete within ~200 fs, indicating that the initial sequential two-photon state has a short lifetime. At the same time, the average vibrational kinetic energy of the tetrazine ring portion of $TzCl_2$ increases substantially, while the average kinetic energy of the chlorine substituents remains relatively unchanged. The vibrational energy is selectively directed into the tetrazine ring, supporting the experimentally observed photochemistry.

The relaxation process in PetrinTzCl is shown in Figure 11. Here, the vibrational relaxation is more complex as the excess electronic energy can be dissipated into the tetrazine portion or the Petrin portion of the molecule. The evolution of the S_1 excess electronic energy and the contributions to the vibrational kinetic energy from the tetrazine ring and the Petrin group for the single representative trajectory in which ring-opening occurs is shown in Figure 11 (top) for one trajectory. Here, the system returns to S_1 within ~15 fs, and the dissipated energy is transferred to vibrational motion in the tetrazine ring. The kinetic energy of the tetrazine ring shows a dramatic increase corresponding to the decrease in excess potential energy.

DOI: 10.1021/acs.jpca.5b02092
J. Phys. Chem. A 2015, 119, 4846−4855

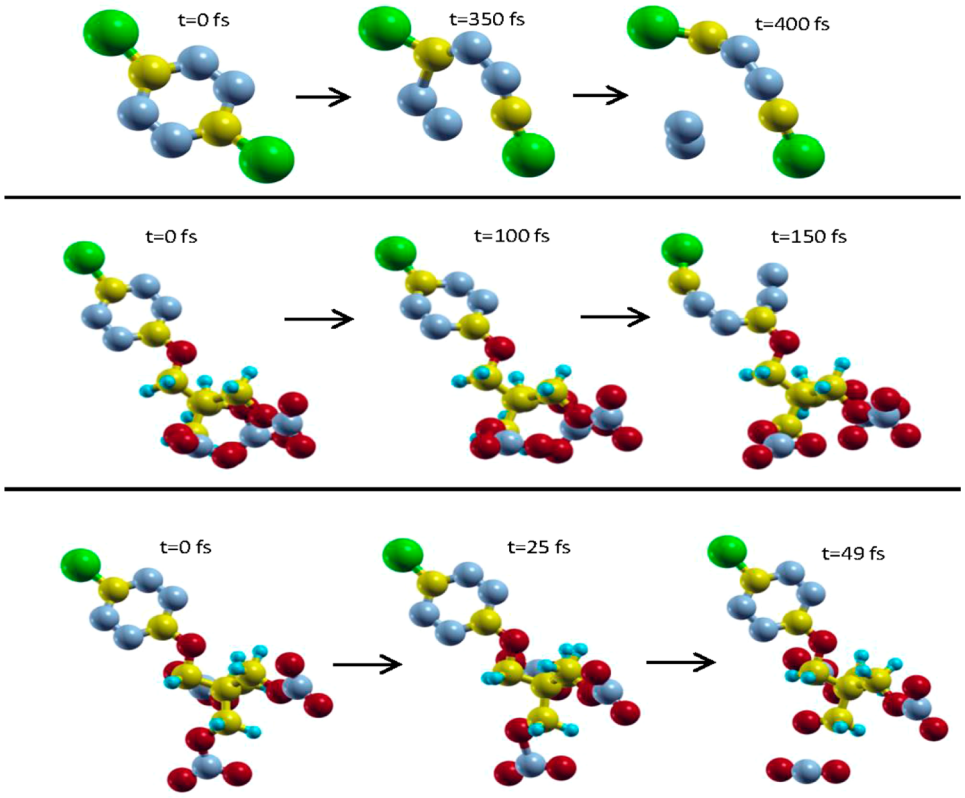

Figure 9. Molecular configurations along representative NA-ESMD trajectories demonstrating photochemistry. (top) $TzCl_2$ tetrazine ring-opening and subsequent release of N_2. (middle) Tetrazine ring-opening in PetrinTzCl. (bottom) NO_2 dissociation from the Petrin functional group in PetrinTzCl.

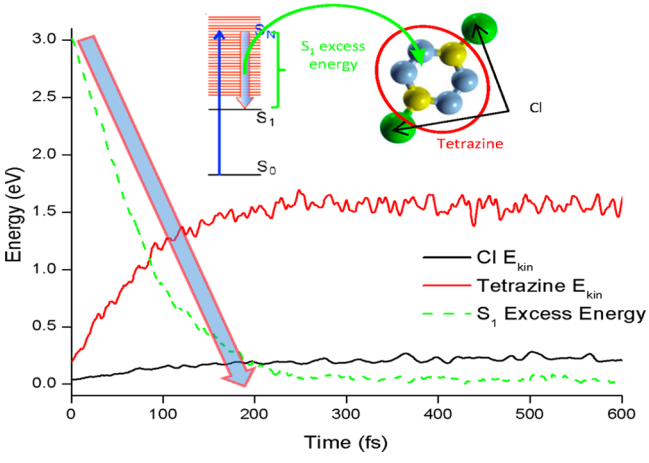

Figure 10. Evolution of the average excess electronic energy and vibrational kinetic energy contributions from tetrazine ring and chlorine substituents for $TzCl_2$ NA-ESMD simulations.

Meanwhile, the kinetic energy of the Petrin fragment remains relatively unchanged. Figure 11 (bottom) displays the same quantities averaged over the simulated ensemble of trajectories that undergo NO_2 dissociation from the Petrin group. In that case, the electronic relaxation to S_1 is complete within 100 fs, suggesting a short lifetime of the initially excited sequential two-photon tetrazine state, and the dissipated electronic energy is preferentially transferred to the Petrin group leaving the tetrazine ring with very little vibrational kinetic energy and increasing only the vibrational kinetic energy of the Petrin fragment.

s-Tetrazine, having a photochemical quantum yield of unity, has been studied mechanistically for some time.[5,48] Two mechanisms have been suggested: either decomposition through IC to a vibrationally excited ground state after one-photon absorption to S_1 or sequential absorption of two photons and subsequent photodecomposition through IC to the S_1 surface.[5,48,51] Our theoretical and experimental results suggest that photochemical decomposition of $TzCl_2$ and PetrinTzCl can occur through sequential two-photon absorption to higher lying excited states and rapid IC to the S_1 excited state.

In simulations, dissociation of NO_2 occurs in PetrinTzCl at a higher calculated quantum yield than ring-opening of the tetrazine moiety. It is important to note that nonadiabatic simulations do not include the possibility for IC to occur from S_1 to the ground state, which may involve an increase in the yield of tetrazine chemistry. It is also possible that dissociation of NO_2 could result in the NO observed in experimental measurements. On the other hand, the Petrin moiety may provide a deactivation mechanism for the excited state rather than an additional photochemical pathway. This discrepancy between theory and experiment could be due to the lack of an effective medium in quantum chemical simulations and/or caging effects in nanocrystalites of PetrinTzCl in experiment, effectively prohibiting NO_2 dissociation. In either case, it seems that the reduced photochemical quantum yield in PetrinTzCl versus $TzCl_2$ is due to an alternative pathway presented by the Petrin moiety.

DOI: 10.1021/acs.jpca.5b02092
J. Phys. Chem. A 2015, 119, 4846−4855

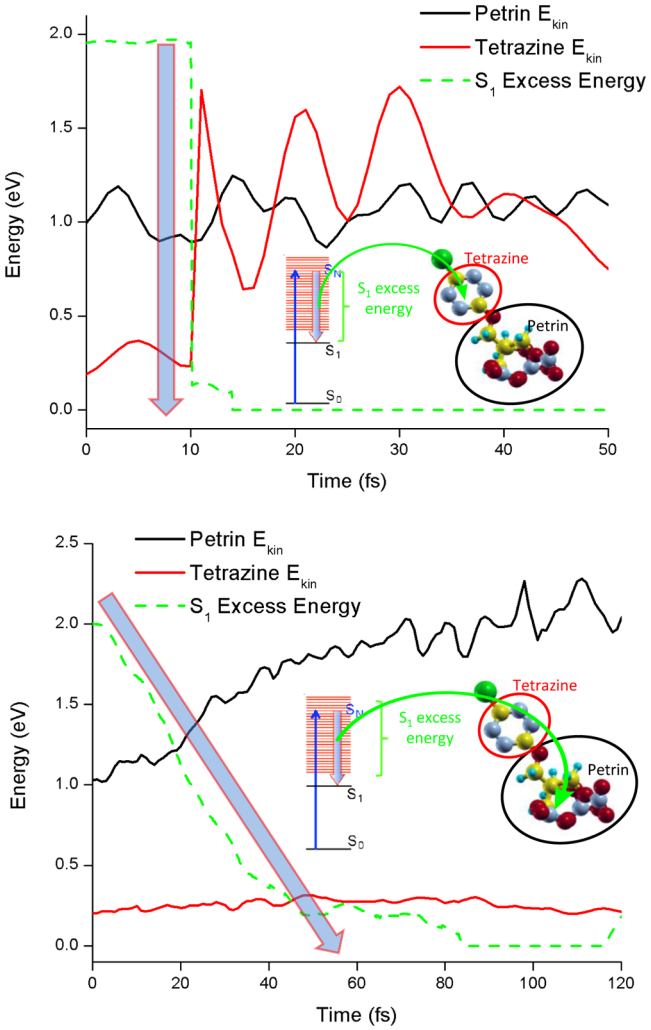

Figure 11. Evolution of the excess electronic energy and vibrational kinetic energy contributions from tetrazine ring and Petrin fragment for PetrinTzCl NA-ESMD simulations. (top) A representative trajectory in which ring-opening is observed and (bottom) average energy for the ensemble of trajectories exhibiting NO_2 dissociation.

CONCLUSIONS

PETN, a conventional high explosive, is not optically active in the visible. The energetic Tz chromophore has been successfully synthetically coupled to PETN increasing its photoactivity at the commonly available laser wavelength of 532 nm. This derivatized material, PetrinTzCl, follows a multiphoton intensity dependent 532 nm absorption that increases its photon quantum yield by 19 times at the maximum intensity employed here, which is easily achieved by small nanosecond lasers. The high-intensity photodecomposition primarily follows a Tz ring photodecomposition, which yields Cl−CN, Petrin−CN, and N_2. Theoretical calculations on two-photon absorption confirm the resonant cascaded process is dominant at the intensities employed. The two-photon cascaded absorption is highly selective allowing the system to access electronic states that are otherwise inaccessible through linear one-photon absorption. NA-ESMD calculations suggest that reaction occurs due to ultrafast (∼100−200 fs) internal conversion where the excess electronic energy from the highly excited sequential two-photon state is dissipated into vibrational kinetic energy as the system relaxes to S_1. The addition of Petrin to the energetic tetrazine chromophore stabilizes the tetrazine, making it more stable to ambient light, while maintaining the potential to initiate photochemistry through multiphoton processes with intense pulsed light. These insights are suggestive for design of the future generation of functional photoactive high explosives initiated optically.

ASSOCIATED CONTENT

Supporting Information

Table containing the values for the computed excitation energies and oscillator strengths for one photon absorption from S_0 or S_1 to S_n; the measured fluorescence emission spectra of 1.4×10^{-4} M solution of PetrinTzCl in acetone excited with a continuous wave 405 nm, 89.8 ± 0.2 mW diode laser; and the simulated two-photon absorption (TPA) of PetrinTzCl in units of Goeppert−Meyers (GM). The Supporting Information is available free of charge on the ACS Publications website at DOI: 10.1021/acs.jpca.5b02092.

AUTHOR INFORMATION

Corresponding Authors

*E-mail serg@lanl.gov (S.T.).
*E-mail scharff@lanl.gov (R.J.S.).

Notes

The authors declare no competing financial interest.

ACKNOWLEDGMENTS

The authors thank the Los Alamos National Laboratory (LANL) Directed Research and Development funds. LANL is operated by Los Alamos National Security, LLC, for the National Nuclear Security Administration of the U.S. Department of Energy under Contract DE-AC52-06NA25396. We acknowledge support of Center for Integrated Nanotechnology (CINT) and Center for Nonlinear Studies (CNLS) at LANL. Additionally, the authors thank David E. Chavez, Jacqueline M. Veauthier, and Susan Hanson for providing the PetrinTzCl and $TzCl_2$.

REFERENCES

(1) Zhou, Y.; Long, X.; Shu, Y. Theoretical Studies on the Heats of Formation, Densities, and Detonation Properties of Substituted s-Tetrazine Compounds. *J. Mol. Model.* **2010**, *16*, 1021−1027.
(2) Chavez, D. E.; Hanson, S. K.; Veauthier, J. M.; Parrish, D. A. Electroactive Explosives: Nitrate Ester-Functionalized 1,2,4,5-Tetrazines. *Angew. Chem., Int. Ed.* **2013**, *52*, 6876−6879.
(3) Li, Z.; Ding, J. F.; Song, N. H.; Du, X. M.; Zhou, J. Y.; Lu, J. P.; Tao, Y. Alternating Copolymers of Dithienyl-s-Tetrazine and Cyclopentadithiophene for Organic Photovoltaic Applications. *Chem. Mater.* **2011**, *23*, 1977−1984.
(4) Hochstrasser, R. M.; King, D. S.; Smith, A. B. Spectroscopy, Photophysics, and Photochemistry of Dimethyl-s-Tetrazine and Phenyl-s-Tetrazine in Crystals and Mixed Crystals at Low Temperatures. *J. Am. Chem. Soc.* **1977**, *99*, 3923−3933.
(5) Hochstrasser, R. M.; King, D. S. Isotopically Selective Spectroscopy and Photochemistry of Sigma-Tetrazine in Crystals and Mixed Crystals at Low Temperature. *J. Am. Chem. Soc.* **1976**, *98*, 5443−5450.
(6) Gong, Y.-H.; Miomandre, F.; Meallet-Renault, R.; Badre, S.; Galmiche, L.; Tang, J.; Audebert, P.; Clavier, G. Synthesis and Physical Chemistry of s-Tetrazines: Which Ones are Fluorescent and Why? *Eur. J. Org. Chem.* **2009**, 6121−6128.
(7) Tucker, M. J.; Courter, J. R.; Chen, J.; Atasoylu, O.; Smith, A. B.; Hochstrasser, I. I. I.; Tetrazine Phototriggers, R. M. Probes for Peptide Dynamics. *Angew. Chem., Int. Ed.* **2010**, *49*, 3612−3616.

(8) Jaiswal, S.; Varma, P. C. R.; O'Neill, L.; Duffy, B.; McHale, P. An Investigation of the Biochemical properties of Tetrazines as Potential Coating Additives. *Mater. Sci. Eng., C* **2013**, *33*, 1925−1934.
(9) Rossin, R.; Verkerk, P. R.; van den Bosch, S. M.; Vulders, R. C. M.; Verel, I.; Lub, J.; Robillard, M. S. In Vivo Chemistry for Pretargeted Tumor Imaging in Live Mice. *Angew. Chem., Int. Ed.* **2010**, *49*, 3375−3378.
(10) Devaraj, N. K.; Upadhyay, R.; Hatin, J. B.; Hilderbrand, S. A.; Weissleder, R. Fast and Sensitive Pretargeted Labeling of Cancer Cells through a Tetrazine/trans-Cyclooctene Cycloaddition. *Angew. Chem., Int. Ed.* **2009**, *48*, 7013−7016.
(11) Lu, Z.-Z.; Zhang, R.; Li, Y.-Z.; Guo, Z.-J.; Zheng, H.-G. Solvatochromic Behavior of a Nanotubular Metal-Organic Framework for Sensing Small Molecules. *J. Am. Chem. Soc.* **2011**, *133*, 4172−4174.
(12) Ponnu, A.; Anslyn, E. V.; Fuorescence-Based, A. Cyclodextrin Sensor to Detect Nitroaromatic Explosives. *Supramol. Chem.* **2010**, *22*, 65−71.
(13) Zhao, Y.; Li, Y.; Qin, Z.; Jiang, R.; Liu, H.; Li, Y. Selective and Colorimetric Fluoride Anion Chemosensor Based on s-Tetrazines. *Dalton Trans.* **2012**, *41*, 13338−13342.
(14) Kulys, J.; Palaima, A.; Urbelis, G. Employing Heterocyclic Dihydropolyazines for Amperometric Glucose Sensing. *Anal. Lett.* **1998**, *31*, 569−584.
(15) Audebert, P.; Miomandre, F.; Clavier, G.; Vernieres, M. C.; Badre, S.; Meallet-Renault, R. Synthesis and Properties of New Tetrazines Substituted by Heteroatoms: Towards the World's Smallest Organic Fluorophores. *Chem.—Eur. J.* **2005**, *11*, 5667−5673.
(16) Oxley, J. C.; Smith, J. L.; Chen, H. Thermal Decomposition of High-Nitrogen Energetic Compounds - Dihydrazido-S-Tetrazine Salts. *Thermochim. Acta* **2002**, *384*, 91−99.
(17) Chavez, D. E.; Gilardi, R. D. Synthesis of 3,6-Bis(3-azido-1,2,4-triazol-1-yl)-1,2,4,5-tetrazine. *J. Energy Mater.* **2009**, *27*, 110−117.
(18) Chavez, D. E.; Parrish, D. A. New Heterocycles from Tetrazines and Oxadiazoles. *J. Heterocycl. Chem.* **2009**, *46*, 88−90.
(19) Aluker, E. D.; Krechetov, A. G.; Mitrofanov, A. Y.; Nurmukhametov, D. R. Photochemical and Photothermal Dissociation of PETN during Laser Initiation. *Russ. J. Phys. Chem. B* **2011**, *5*, 658−660.
(20) Aluker, E. D.; Belokurov, G. M.; Krechetov, A. G.; Mitrofanov, A. Y.; Nurmukhametov, D. R. Laser Initiation of PETN Containing Light-Scattering Additives. *Technol. Phys. Lett.* **2010**, *36*, 285−287.
(21) Aduev, B. P.; Nurmukhametov, D. R.; Puzynin, A. V. Laser Initiation of a Mixture of PETN with NiC Nanoparticles at Elevated Temperatures. *Russ. J. Phys. Chem. B* **2010**, *4*, 452−456.
(22) Stewart, D. S.; Thomas, K. A.; Clarke, S.; Mallett, H.; Martin, E.; Martinez, M.; Munger, A.; Saenz, J. On the Initiation Mechanism in Exploding Bridgewire and Laser Detonators. *AIP Conf. Proc.* **2006**, *845*, 471−474.
(23) Akinci, A.; Thomas, K.; Munger, A.; Nunn, L.; Clarke, S.; Johnson, M.; Kennedy, J.; Montoya, D. On the Development of a Laser Detonator. *Proc. SPIE* **2005**, *5871*, 1−7.
(24) Nagayama, K.; Inou, K.; Nakahara, M. Initiation of PETN High Explosive by Pulse Laser-Induced High-Temperature Plasma. In *Impact Engineering and Application*; Chiba, A., Tanimura, S., Hokamoto, K., Eds.; 2001; Vols. *I* and *II*, pp 515−519.
(25) Tarzhanov, V. I.; Zinchenko, A. D.; Sdobnov, V. I.; Tokarev, B. B.; Pogrebov, A. I.; Volkova, A. A. Laser Initiation of PETN. *Combust., Explos. Shock Waves* **1996**, *32*, 454−459.
(26) Bykhalo, A. I.; Zhuzhukalo, E. V.; Kovalskii, N. G.; Kolomiiskii, A. N.; Korobov, V. V.; Rozhkov, A. D.; Yudin, A. I. Initiation of PETN by High-Power Laser Radiation. *Combust., Explos. Shock Waves* **1985**, *21*, 481−483.
(27) Brouwer, A. M. Standards or Photoluminescence Quantum Yield Measurements in Solution (IUPAC Technical Report). *Pure Appl. Chem.* **2011**, *83*, 2213−2228.
(28) NIST Chemistry WebBook; http://webbook.nist.gov/chemistry/ (accessed 01/12/15).
(29) Frisch, M. J.; Trucks, G. W.; Schlegel, H. B.; Scuseria, G. E.; Robb, M. A.; Cheeseman, J. R.; Montgomery, J. J. A.; Vreven, T.; Kudin, K. N.; Burant, J. C.; et al. *Gaussian 03, Rev. E*; Gaussian Inc.: Wallingford, CT, 2004.
(30) Frisch, M. J.; Trucks, G. W.; Schlegel, H. B.; Scuseria, G. E.; Robb, M. A.; Cheeseman, J. R.; Scalmani, G.; Barone, V.; Mennucci, B.; Petersson, G. A.; et al. *Gaussian 09, Rev. B*; Gaussian Inc.: Wallingford, CT, 2009.
(31) Masunov, A. M.; Tretiak, S. Prediction of Two-Photon Absorption Properties for Organic Chromophores Using Time-Dependent Density-Functional Theory. *J. Phys. Chem. B* **2004**, *108*, 899−907.
(32) El-Azhary, A. A.; Suter, H. U. Comparison Between Optimized Geometries and Vibrational Frequencies Calculated by the DFT Methods. *J. Phys. Chem.* **1996**, *100*, 15056−15063.
(33) Terenziani, F.; Katan, C.; Badaeva, E.; Tretiak, S.; Blanchard-Desce, M. Enhanced Two-Photon Absorption of Organic Chromophores: Theoretical and Experimental Assessments. *Adv. Mater.* **2008**, *20*, 4641−4678.
(34) Tretiak, S.; Chernyak, V. Resonant Nonlinear Polarizabilities in the Time-Dependent Density Functional Theory. *J. Chem. Phys.* **2003**, *119*, 8809−8823.
(35) Nelson, T.; Fernandez-Alberti, S.; Chernyak, V.; Roitberg, A. E.; Tretiak, S. Nonadiabatic Excited-State Molecular Dynamics Modeling of Photoinduced Dynamics in Conjugated Molecules. *J. Phys. Chem. B* **2011**, *115*, 5402−5414.
(36) Fernandez-Alberti, S.; Roitberg, A. E.; Nelson, T.; Tretiak, S. Identification of Unavoided Crossings in Nonadiabatic Photoexcited Dynamics Involving Multiple Electronic States in Polyatomic Conjugated Molecules. *J. Chem. Phys.* **2012**, *137*, 014512.
(37) Nelson, T.; Fernandez-Alberti, S.; Chernyak, V.; Roitberg, A. E.; Tretiak, S. Nonadiabatic Excited-State Molecular Dynamics: Numerical Tests of Convergence and Parameters. *J. Chem. Phys.* **2012**, *136*, 054108.
(38) Nelson, T.; Fernandez-Alberti, S.; Roitberg, A. E.; Tretiak, S. Nonadiabatic Excited-State Molecular Dynamics: Treatment of Electronic Decoherence. *J. Chem. Phys.* **2013**, *138*, 224111.
(39) Nelson, T.; Fernandez-Alberti, S.; Roitberg, A. E.; Tretiak, S. Nonadiabatic Excited-State Molecular Dynamics: Modeling Photophysics in Organic Conjugated Materials. *Acc. Chem. Res.* **2014**, *47*, 1155−1164.
(40) Tully, J. C. Molecular Dynamics with Electronic Transitions. *J. Chem. Phys.* **1990**, *93*, 1061−1071.
(41) Thouless, D. J. *The Quantum Mechanics Of Many-Body Systems*; Academic Press: New York, 1972.
(42) Dewar, M. J. S.; Zoebisch, E. G.; Healy, E. F.; Stewart, J. J. P. Development and Use of Quantum Mechanical Molecular Models. 76. AM1: A New General Purpose Quantum Mechanical Molecular Model. *J. Am. Chem. Soc.* **1985**, *107*, 3902−3909.
(43) Paterlini, M.; Ferguson, D. Constant Temperature Simulations using the Langevin Equation with Velocity Verlet Integration. *Chem. Phys.* **1998**, *236*, 243−252.
(44) Waluk, J.; Spangetlarsen, J.; Thulstrup, E. W. Electronic States of Symmetrically Disubstituted s-Tetrazines. *Chem. Phys.* **1995**, *200*, 201−213.
(45) Zhou, Q. *Synthesis of New Tetrazines Functionalized with Photoactive and Electroactive Groups*; Ecole normale supérieure de Cachan, 2012.
(46) Guckel, F.; Maki, A. H.; Neugebauer, F. A.; Schweitzer, D.; Vogler, H. Spectroscopic Investigations of the Lowest Triplet State of s-Tetrazines. *Chem. Phys.* **1992**, *164*, 217−227.
(47) Tucker, M. J.; Abdo, M.; Courter, J. R.; Chen, J.; Smith, A. B., III; Hochstrasser, R. M. Di-Cysteine S,S-Tetrazine: A Potential Ultrafast Photochemical Trigger to Explore the Early Events of Peptide/Protein Folding. *J. Photochem. Photobiol., A* **2012**, *234*, 156−163.
(48) Zhao, X. S.; Miller, W. B.; Hintsa, E. J.; Lee, Y. T. A Concerted Triple Dissociation—The Photochemistry of s-Tetrazine. *J. Chem. Phys.* **1989**, *90*, 5527−5535.

DOI: 10.1021/acs.jpca.5b02092
J. Phys. Chem. A 2015, 119, 4846−4855

(49) Guo, Y.; Bhattacharya, A.; Bernstein, E. R. Decomposition of Excited Electronic State s-Tetrazine and Its Energetic Derivatives. *J. Chem. Phys.* **2011**, *134*, 024318.
(50) Scheiner, A. C.; Scuseria, G. E.; Schaefer, H. F. Mechanism of the Photodissociation of s-Tetrazine: A Unimolecular Triple Dissociation. *J. Am. Chem. Soc.* **1986**, *108*, 8160−8162.
(51) Haynam, C. A.; Brumbaugh, D. V.; Levy, D. H. The Spectroscopy, Photophysics, and Photochemistry of the Dimer of Dimethyl Tetrazine. *J. Chem. Phys.* **1984**, *81*, 2282−2294.

DOI: 10.1021/acs.jpca.5b02092
J. Phys. Chem. A 2015, 119, 4846−4855